JACS
JOURNAL OF THE AMERICAN CHEMICAL SOCIETY

Communication

pubs.acs.org/JACS

Observation of Internal Photoinduced Electron and Hole Separation in Hybrid Two-Dimentional Perovskite Films

Junxue Liu,[†,‡,§] Jing Leng,[†,‡] Kaifeng Wu,[‡] Jun Zhang,[*,§] and Shengye Jin[*,‡]

[‡]State Key Laboratory of Molecular Reaction Dynamics and Collaborative Innovation Center of Chemistry for Energy Materials (iChEM), Dalian Institute of Chemical Physics, Chinese Academy of Sciences, 457 Zhongshan Road, Dalian 116023, China

[§]State Key Laboratory of Heavy Oil Processing, College of Chemical Engineering, China University of Petroleum, 66 Changjiang West Road, Huangdao District, Qingdao 266580, China

Supporting Information

ABSTRACT: Two-dimensional (2D) organolead halide perovskites are promising for various optoelectronic applications. Here we report a unique spontaneous charge (electron/hole) separation property in multilayered $(BA)_2(MA)_{n-1}Pb_nI_{3n+1}$ (BA = $CH_3(CH_2)_3NH_3^+$, MA = $CH_3NH_3^+$) 2D perovskite films by studying the charge carrier dynamics using ultrafast transient absorption and photoluminescence spectroscopy. Surprisingly, the 2D perovskite films, although nominally prepared as "n = 4", are found to be mixture of multiple perovskite phases, with n = 2, 3, 4 and $\approx \infty$, that naturally align in the order of n along the direction perpendicular to the substrate. Driven by the band alignment between 2D perovskites phases, we observe consecutive photoinduced electron transfer from small-n to large-n phases and hole transfer in the opposite direction on hundreds of picoseconds inside the 2D film of ~358 nm thickness. This internal charge transfer efficiently separates electrons and holes to the upper and bottom surfaces of the films, which is a unique property beneficial for applications in photovoltaics and other optoelectronics devices.

Two-dimensional (2D) organolead halide perovskites, in addition to their three-dimensional (3D) analogues, have recently emerged as an attractive material for applications in photovoltaics and other optoelectronic devices.[1−16] The structural formula of the 2D perovskite is generally given as $(A)_2(CH_3NH_3)_{n-1}M_nX_{3n+1}$, where A is a large aliphatic or aromatic alkylammonium cation working as an insulating layer, M is the metal cation and X is the halide anion. The integer n is the number of inorganic perovskite layers between two organic cation spacers (A). Due to the geometric effect and dielectric contrast effect, the exciton binding energy in 2D perovskites is much larger than that in 3D perovskites;[17−23] and continuous tunability in exciton absorption/emission energy can be achieved by changing the number of n through quantum confinement effect. These properties have led to successful applications of 2D perovskites in light-harvesting and emitting devices.[6−10] Moreover, using the large organic cations in 2D perovskites can also dramatically improve their moisture resistance,[1−5] making this class of materials more attractive for long-term use in real-life devices.

The applications of 2D perovskites in various devices have immediately triggered many fundamental studies focusing on the carrier dynamics in single-phase 2D crystals and hybrid 2D films.[24−27] Interestingly, recent reports have demonstrated that the 2D multilayered perovskite films actually comprised multiple perovskite phases (with various n values from 1, 2, 3 and 4 to near ∞),[6,7] even though the films were intended to be prepared as a single-phase. This hybrid feature seems to be ineluctable in fabricating 2D films. Because of the band alignment between perovskites with various n values,[1,7] the hybrid structure in 2D films should induce more complicated internal charge carrier transportation than in 3D perovskites where intrinsic carrier diffusion dominates.

Recently, Sargent et al. and Huang et al. have reported the carrier funneling from small-n to large-n perovskite phases in hybrid 2D films, presumably driven by exciton energy transfer.[6,7] However, two important questions remain yet-to-be-answered: first, how the different perovskite phases align in the hybrid films; second, whether the band alignment between different phases induces energy funneling as reported in ref 6, 7 or instead charge separation. The latter is especially important because it dictates the application of these hybrid 2D perovskite films: energy funneling is useful for light-emitting applications, whereas charge separation would be more beneficial for light conversion or detection.

Herein, using ultrafast transient absorption (TA) and time-resolved photoluminescence (PL) spectroscopy we studied the charge carrier dynamics in $(BA)_2(MA)_{n-1}Pb_nI_{3n+1}$ 2D perovskite films (BA = $CH_3(CH_2)_3NH_3^+$, MA = $CH_3NH_3^+$). We found that indeed multiple perovskite phases with various n values coexisted in the 2D perovskite films (although nominally prepared as "n = 4"), and more interestingly, these perovskite phases were naturally aligned in the order of n along the growth direction perpendicular to the substrate. Driven by the built-in band alignment between different perovskite phases, consecutive internal electron transfer (with a time of ~477 ps) from small-n to large-n perovskite phases and hole transfer (with a time of ~987 ps) in the opposite direction were observed in a film of ~358 nm thickness. This unique self-charge-separation property of the 2D perovskite films can facilitate their applications in photovoltaics and other optoelectronics devices.

Received: December 7, 2016
Published: January 17, 2017

DOI: 10.1021/jacs.6b12581
J. Am. Chem. Soc. 2017, 139, 1432−1435

The 2D perovskite films were prepared by spin-coating a precursor solution of $CH_3(CH_2)_3NH_3I$ (BAI), CH_3NH_3I (MAI) and PbI_2 with a molar ratio of 2:3:4 dissolved in *N*,*N*-dimethylformamide (DMF) via a hot-casting process (see SI for details and Figure S1 for SEM images).[2] The precursor mixtures crystallize to form perovskite phases when DMF solvent evaporates. The molar ratio of precursor corresponds to a nominal composition of $(BA)_2(MA)_3Pb_4I_{13}$ (n = 4). Figure 1a shows the UV−vis absorption spectrum of a typical 2D perovskite film. In addition to the lowest bandgap absorption at ∼740 nm (1.68 eV), three higher energy absorption peaks, at ∼572 nm (2.17 eV), 608 nm (2.04 eV) and ∼645 nm (1.93 eV), are also found in the spectrum. Comparing with the absorption of 2D-perovskite single crystals (Figure S2), the high energy absorption peaks at ∼572, 608 and 645 nm can be assigned to single-phase $(BA)_2(MA)_{n-1}Pb_nI_{3n+1}$ perovskites with n = 2, 3 and 4, respectively. The lowest absorption peak at 740 nm, which is close to the 3D perovskite, corresponds to a (or a group of) perovskite phase(s) with much larger n values ($n \approx \infty$). This result suggests that the 2D perovskite films comprise hybrid perovskite phases with different n values, even though the molar ratio of used precursors is intended for a single phase perovskite with n = 4. This hybrid feature of the 2D perovskite film is consistent with recently reported films fabricated by similar methods.[6,7]

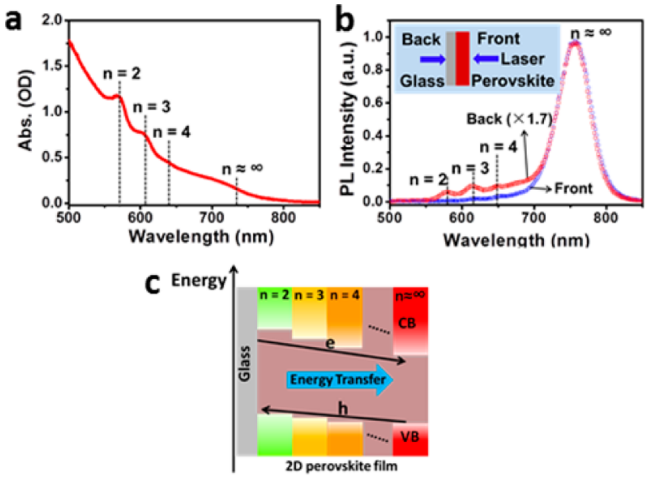

Figure 1. (a) UV−vis absorption spectrum of a typical $(BA)_2(MA)_{n-1}Pb_nI_{3n+1}$ 2D perovskite film (∼358 nm thickness, prepared as n = 4). The perovskite film exhibited multiple absorption peaks, which are identified as n = 2 (2.17 eV), n = 3 (2.04 eV), n = 4 (1.93 eV) and $n \approx \infty$ perovskite phases. (b) Comparison of the emission spectra of the 2D perovskite film illuminated from the front and back sides (as illustrated in the inset) of the film. Under back-excitation, the spectrum show emission peaks from n = 2, 3 and 4 phases in addition to the dominant emission from $n \approx \infty$ phase. (c) Comparative bandgap energy alignment of $(BA)_2(MA)_{n-1}Pb_nI_{3n+1}$ perovskites with different n values. Three possible carrier transfer mechanisms, electron and energy transfers from small-n to large-n perovskites and hole transfer from large-n to small-n perovskites, are all energetically allowed.

To examine whether these different perovskite phases distribute randomly or follow a specific order, the photoluminescence (PL) spectra of the 2D perovskite film were collected under two different excitation configurations (Figure 1b). The configuration with the laser beam (405 nm) impinging the perovskite (or the glass substrate) is defined as the front (or back) excitation (see the inset in Figure 1b). The spectra with both excitations show a dominant emission peak at ∼750 nm ($n \approx \infty$); however, under back-excitation three emission peaks at higher energy were observed, which can be attributed to the emission from the perovskite phases with n = 2, 3 and 4. The difference in the PL spectra between back- and front-excitations implies that the small-n phases should majorly locate at the bottom surface and the large-n phase locates at the upper surface of the film. Our TA measurements that will be discussed below further confirm that the different perovskite phases distribute in the order of their n values (from n = 2 at the bottom surface to $n \approx \infty$ at the upper surface). The reason for forming this sequentially distributed perovskite phases is unclear. We propose that in fabricating the films the local molar ratio of BAI insulating cations to MAI and PbI_2 precursors likely changes during the DMF solvent evaporation process, leading to different local n values in perovskite crystallization.

Because the perovskites with different n values exhibit a certain band alignment, it is expected that the ordered distribution of perovskite phases should prompt directional carrier transportation inside the film. In Figure 1c, we show the bandgap diagram of the perovskite phases found in our films using the reported valence band (VB) and conduction band (CB) positions of 2D perovskites with n = 2 to 4 and 3D perovskite.[1,7] Based on the band alignment, photoinduced electron transfer from small-n to large-n perovskites and hole transfer in the opposite direction are both energetically allowed. Furthermore, because of the spectral overlap between the emission of small-n perovskites and the absorption of large-n perovskites, energy transfer from small-n to large-n perovskites is also possible in the hybrid film.

To elucidate the interaction mechanism between different-n perovskite components, we investigated the charge carrier dynamics in the hybrid 2D perovskite films using the femtosecond transient absorption (TA) and time-resolved PL spectroscopy. For TA measurements, a pump pulse was used to excite the perovskite films and the induced absorption changes (ΔA), as functions of both wavelength and time, were recorded. Figure 2a shows the TA spectra at the indicated delay times of the 2D perovskite film (358 nm thickness) under back-excitation (at 480 nm, 0.7 $\mu J/cm^2$/pulse). Consistent with the static absorption spectrum, the TA spectra exhibit four bleach peaks at n = 2, 3, 4 and $n \approx \infty$ absorption bands due to the charge carrier filling upon excitation. A small bleach peak between the n = 4 and $n \approx \infty$ bands is identified as the n = 5 perovskite phase (see Figure S2) whose absorption peak is likely hidden in the broad absorption signal of $n \approx \infty$ component. For comparison, the TA spectra of the same film with the front-excitation are shown in Figure 2b, where the TA spectra are dominated by the bleach signals from the $n \approx \infty$ phase. This difference in TA spectra between back- and front-excitations agrees with the observation in the PL spectra.

Under back-excitation, we observed that the bleach recovery at n = 2, 3 and 4 is accompanied by the formation of the $n \approx \infty$ species (Figure 2a). Such a process is also observed under front-excitation at very early delay times (Figure 2b), when the small-n phases are excited by photons penetrating through the $n \approx \infty$ phase. This result suggests the charge carrier transportation from the small-n phases to $n \approx \infty$ in the film. The TA kinetics probed at these bands are shown in Figure 2c. The bleach recovery kinetics (after subtracting the photoinduced absorption (PIA) signal from the $n \approx \infty$ phase) becomes slower as the n value increases, and a rising kinetics appears for the $n \approx \infty$ band, indicating carrier accumulation on this perovskite phase. The

DOI: 10.1021/jacs.6b12581
J. Am. Chem. Soc. 2017, 139, 1432−1435

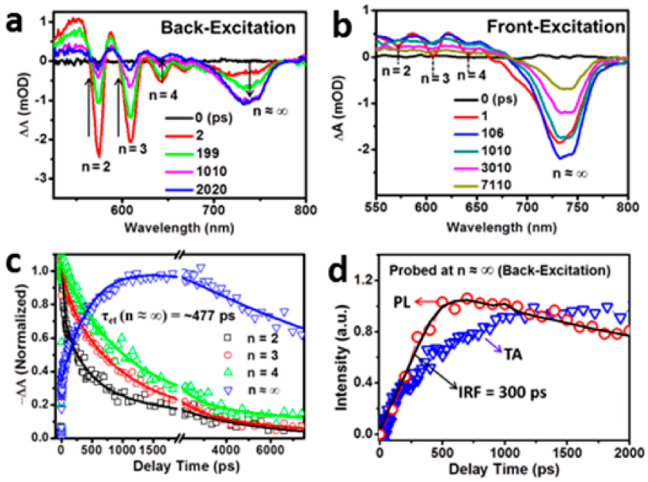

Figure 2. TA spectra at different delay times of a typical $(BA)_2(MA)_{n-1}Pb_nI_{3n+1}$ 2D perovskite film (~358 nm thickness, prepared as $n = 4$) under (a) back- and (b) front-excitations. Bleach peaks formed by carrier band edge filling at 572, 608, 645 and 740 nm are identified as $n = 2$, 3, 4 and $n \approx \infty$ perovskite phases, respectively. Black arrows indicate the direction of the bleach peak evolution. (c) TA kinetics probed at $n = 2$, 3, 4 and $n \approx \infty$ bands under back-excitation. The slow rising kinetics at $n \approx \infty$ band reflects the carrier (electron) populating process to this phase. Solid lines are the fits of the kinetics by exponential function, which yields the carrier populating time of 477 ps. (d) Comparison of the time-resolved PL and TA kinetics traces probed at the $n \approx \infty$ band in the first two nanoseconds after excitation, showing clear discrepancy in the rising kinetics. The solid line is the fit of the PL kinetics with the rising kinetics limited by the IRF.

trend in these TA kinetics can be explained by the consecutive carrier transfer through the perovskite phases, which should be sequentially distributed in the order of n values in the film. Such sequential alignment of perovskite phases and the corresponding consecutive carrier transportation are further confirmed in a 2D perovskite film with a larger thickness of ~523 nm (Figure S3 and S4).

According to the diagram in Figure 1c, carrier transportation from small-n to $n \approx \infty$ phases could result from electron or energy transfers. In the latter case, the carrier (exciton) accumulation at the $n \approx \infty$ band observed in TA measurements should be also seen in the time-resolved PL kinetics. To differentiate these two mechanisms, we compared the TA kinetics (probed at the $n \approx \infty$ band) and the transient PL trace (collected under back-excitation at 750 nm) (Figure 2d). It is clear that the rising kinetics in TA is slower than the rising component in the PL trace (where the rising kinetics is determined by the instrument response function (IRF = ~300 ps)), indicating that carrier populating process in these two measurements are different. This discrepancy between TA and PL kinetics was also observed in the thicker (523 nm) 2D film (Figure S4d). On the basis of these results, we confirm that the carrier transfer from small-n to $n \approx \infty$ perovskite phases should be attributed to the electron transfer rather than the energy transfer. The observed PL from the $n \approx \infty$ phase should be due to the direct excitation by photons penetrating through small-n phases under back-excitation.

In Figure S5, we also compared the TA kinetics (probed at $n \approx \infty$) in the 2D perovskite films before and after the depositions of PCBM (electron acceptor) and Spiro-OMeTAD (hole acceptor). With PCBM, the charge accumulation process at $n \approx \infty$ band disappears and the kinetics recovers much faster, suggesting the efficient interfacial electron transfer from the $n \approx \infty$ phase to PCBM. In contrast, the TA kinetics in the film with the hole acceptor deposition remains unchanged relative to that of the neat film. This result further confirms the internal electron transfer rather than the energy transfer from small-n to $n \approx \infty$ perovskite phases in the 2D film.

Directionally opposite to the electron transfer, hole transfer from large-n to small-n perovskite components is also energetically allowed. To probe the hole transfer, we performed the TA measurements on the film under front-excitation at 740 nm (3.5 $\mu J/cm^2$/pulse). At this excitation wavelength, only the $n \approx \infty$ perovskite phase should be excited. Figure 3a shows the TA

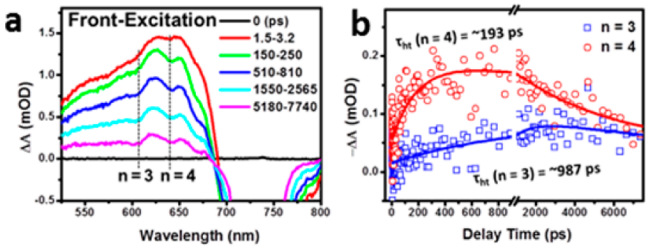

Figure 3. (a) TA spectra of the $(BA)_2(MA)_{n-1}Pb_nI_{3n+1}$ 2D perovskite film (prepared as $n = 4$, ~358 nm thickness) under front-excitation at 740 nm. Bleach peaks at 608 and 645 nm are assigned to the $n = 3$ and 4 perovskite phases. (b) TA kinetics (after subtracting PIA contribution) probed at $n = 3$ and 4 bands showing the bleach formation processes due to the hole transfer from the $n \approx \infty$ phase. Solid lines are the fits of kinetics by exponential function, yielding the hole transfer time of 192 ps to $n = 4$ phase and 987 ps to $n = 3$ phase.

spectra of the film. In addition to the broad PIA signal from $n \approx \infty$ band, two small bleach peaks growing larger at later delay times are observed, and can be assigned to the $n = 3$ and 4 perovskite phases (Figure S6). The TA kinetics probed at these bands (after subtracting the PIA contribution) (Figure 3b) show the bleach formation processes with the times becoming longer from $n = 4$ to $n = 3$ band. These TA results can be well explained by the consecutive hole transfer from $n \approx \infty$ to $n = 4$ and then to $n = 3$ phases. Furthermore, this hole transfer is also confirmed from the fast PL decay (τ = 680 ps) probed at $n \approx \infty$ band (Figure S7). The observation of hole transfer also suggests the absence of energy transfer in the 2D perovskite films.

Noticeably, the amplitudes of bleach peaks formed by hole transfer are smaller than that by electron transfer. This is partially due to the smaller contribution of hole-filling to the TA bleach signal.[28,29] Another possible reason is the presence of hole-trapping states in the perovskite film,[30] which reduces the number of holes during the transfer process; thus, the formation of the bleach peak for $n = 2$ band that requests the longest hole transfer distance is not observed.

By fitting the TA kinetics with simple multiexponential functions (fitting parameters in Table S1 and S2), we estimated the electron transfer time of ~477 ps (Figure 2c) and the hole transfer time of ≥987 ps (Figure 3b) for transportation across the entire film thickness of ~358 nm. The separated electrons and holes exhibited a longer lifetime of >14 ns (Table S1 and S2). By comparing the charge transfer times to the intrinsic carrier lifetimes of single-phase 2D perovskites, we estimated the theoretical charge separation efficiency of ≥92% by electron transfer (back-excitation) and ~70% by hole transfer (front-excitation) in the 2D films of 358 nm thickness (see Figure S8). In thicker films (e.g., ~500 nm), the charge separation efficiency

DOI: 10.1021/jacs.6b12581
J. Am. Chem. Soc. 2017, 139, 1432−1435

is significantly reduced due to the slower charge transfer process. We also observed that in a thin 2D film of <100 nm thickness the PL quantum yield (PLQY) is enhanced by almost 4−7 times compared to the film of 358 nm thickness (Figure S9b), even though the charge transfer time increase to tens of picoseconds (Figure S10). We proposed that in such a thin film the perovskite phases with different n values are not clearly discrete in space, and electrons and holes do not separate in long distance to suppress their radiative recombination. These results indicate that the thickness of 2D film is a key factor for achieving the high internal charge separation efficiency. Nevertheless, the PLQY of thin 2D perovskite film is still higher than that of 3D film (Figure S9c), which may partially explain the reported better performance of light-emitting diodes using thin (<100 nm) 2D perovskite films.[6,7]

In summary, using static and transient PL and TA spectroscopies we have found that the $(BA)_2(MA)_{n-1}Pb_nI_{3n+1}$ 2D perovskite film comprises hybrid perovskite phases, whose sequential distribution in the order of their n values induced electron and hole transfers occurring in the opposite direction. This internal charge separation can accumulate electrons and holes on the spatially separated upper and bottom surfaces of the films, and thus should principally facilitate the charge extraction to the electrodes when applied in the solar cell. Furthermore, the band energy alignment formed by the sequential distribution of different perovskite components introduces a $p-n$ junction-like property to the 2D perovskite films, paving the way for their novel applications in optoelectronic devices.

■ ASSOCIATED CONTENT

Supporting Information

The Supporting Information is available free of charge on the ACS Publications website at DOI: 10.1021/jacs.6b12581.

Material synthesis; SEM characterization; additional spectroscopic measurements (PDF)

■ AUTHOR INFORMATION

Corresponding Authors

*sjin@dicp.ac.cn

*zhangj@upc.edu.cn

ORCID

Junxue Liu: 0000-0001-8349-1017

Shengye Jin: 0000-0003-2001-2212

Author Contributions

†These authors contributed equally.

Notes

The authors declare no competing financial interest.

■ ACKNOWLEDGMENTS

S.J. acknowledges the financial support from the MOST (2016YFA0200602) and NBRPC (2013CB834604). J.Z. acknowledges the financial support from the NSFC (21471160).

■ REFERENCES

(1) Cao, D. H.; Stoumpos, C. C.; Farha, O. K.; Hupp, J. T.; Kanatzidis, M. G. *J. Am. Chem. Soc.* **2015**, *137*, 7843−7850.

(2) Tsai, H. H.; Nie, W. Y.; Blancon, J. C.; Stoumpos, C. C. S.; Asadpour, R.; Harutyunyan, B.; Neukirch, A. J.; Verduzco, R.; Crochet, J. J.; Tretiak, S.; Pedesseau, L.; Even, J.; Alam, M. A.; Gupta, G.; Lou, J.; Ajayan, P. M.; Bedzyk, M. J.; Kanatzidis, M. G.; Mohite, A. D. *Nature* **2016**, *536*, 312−316.

(3) Smith, I. C.; Hoke, E. T.; Solis-Ibarra, D.; McGehee, M. D.; Karunadasa, H. I. *Angew. Chem., Int. Ed.* **2014**, *53*, 11232−11235.

(4) Quan, L. N.; Yuan, M. J.; Comin, R.; Voznyy, O.; Beauregard, E. M.; Hoogland, S.; Buin, A.; Kirmani, A. R.; Zhao, K.; Amassian, A.; Kim, D. H.; Sargent, E. H. *J. Am. Chem. Soc.* **2016**, *138*, 2649−2655.

(5) Boix, P. P.; Agarwala, S.; Koh, T. M.; Mathews, N.; Mhaisalkar, S. G. *J. Phys. Chem. Lett.* **2015**, *6*, 898−907.

(6) Wang, N.; Cheng, L.; Ge, R.; Zhang, S.; Miao, Y.; Zou, W.; Yi, C.; Sun, Y.; Cao, Y.; Yang, R.; Wei, Y.; Guo, Q.; Ke, Y.; Yu, M.; Jin, Y.; Liu, Y.; Ding, Q.; Di, D.; Yang, L.; Xing, G.; Tian, H.; Jin, C.; Gao, F.; Friend, R. H.; Wang, J.; Huang, W. *Nat. Photonics* **2016**, *10*, 699−704.

(7) Yuan, M.; Quan, L. N.; Comin, R.; Walters, G.; Sabatini, R.; Voznyy, O.; Hoogland, S.; Zhao, Y.; Beauregard, E. M.; Kanjanaboos, P.; Lu, Z.; Kim, D. H.; Sargent, E. H. *Nat. Nanotechnol.* **2016**, *11*, 872−877.

(8) Byun, J.; Cho, H.; Wolf, C.; Jang, M.; Sadhanala, A.; Friend, R. H.; Yang, H.; Lee, T. W. *Adv. Mater.* **2016**, *28*, 7515−7520.

(9) Kumar, S.; Jagielski, J.; Yakunin, S.; Rice, P.; Chiu, Y. C.; Wang, M.; Nedelcu, G.; Kim, Y.; Lin, S.; Santos, E. J.; Kovalenko, M. V.; Shih, C. J. *ACS Nano* **2016**, *10*, 9720−9729.

(10) Zhou, J. C.; Chu, Y. L.; Huang, J. *ACS Appl. Mater. Interfaces* **2016**, *8*, 25660−25666.

(11) Liu, J. Y.; Xue, Y. Z.; Wang, Z. Y.; Xu, Z. Q.; Zheng, C. X.; Weber, B.; Song, J. C.; Wang, Y. S.; Lu, Y. R.; Zhang, Y. P.; Bao, Q. L. *ACS Nano* **2016**, *10*, 3536−3542.

(12) Song, J. Z.; Xu, L. M.; Li, J. H.; Xue, J.; Dong, Y. H.; Li, X. M.; Zeng, H. B. *Adv. Mater.* **2016**, *28*, 4861−4869.

(13) Yao, K.; Wang, X. F.; Xu, Y. X.; Li, F.; Zhou, L. *Chem. Mater.* **2016**, *28*, 3131−3138.

(14) Yang, J.-H.; Yuan, Q.; Yakobson, B. I. *J. Phys. Chem. C* **2016**, *120*, 24682−24687.

(15) Dou, L. T.; Wong, A. B.; Yu, Y.; Lai, M. L.; Kornienko, N.; Eaton, S. W.; Fu, A.; Bischak, C. G.; Ma, J.; Ding, T. N.; Ginsberg, N. S.; Wang, L. W.; Alivisatos, A. P.; Yang, P. D. *Science* **2015**, *349*, 1518−1521.

(16) Dohner, E. R.; Jaffe, A.; Bradshaw, L. R.; Karunadasa, H. I. *J. Am. Chem. Soc.* **2014**, *136*, 13154−13157.

(17) Yaffe, O.; Chernikov, A.; Norman, Z. M.; Zhong, Y.; Velauthapillai, A.; van der Zande, A.; Owen, J. S.; Heinz, T. F. *Phys. Rev. B: Condens. Matter Mater. Phys.* **2015**, *92*, 045414.

(18) Tanaka, K.; Takahashi, T.; Kondo, T.; Umebayashi, T.; Asai, K.; Ema, K. *Phys. Rev. B: Condens. Matter Mater. Phys.* **2005**, *71*, 045312.

(19) Hong, X.; Ishihara, T.; Nurmikko, A. V. *Phys. Rev. B: Condens. Matter Mater. Phys.* **1992**, *45*, 6961−6964.

(20) Ishihara, T. *J. Lumin.* **1994**, *60*−*61*, 269−274.

(21) Tyagi, P.; Arveson, S. M.; Tisdale, W. A. *J. Phys. Chem. Lett.* **2015**, *6*, 1911−1916.

(22) Sichert, J. A.; Tong, Y.; Mutz, N.; Vollmer, M.; Fischer, S.; Milowska, K. Z.; Cortadella, R. G.; Nickel, B.; Cardenas-Daw, C.; Stolarczyk, J. K.; Urban, A. S.; Feldmann, J. *Nano Lett.* **2015**, *15*, 6521−6527.

(23) Malgras, V.; Tominaka, S.; Ryan, J. W.; Henzie, J.; Takei, T.; Ohara, K.; Yamauchi, Y. *J. Am. Chem. Soc.* **2016**, *138*, 13874−13881.

(24) Milot, R. L.; Sutton, R. J.; Eperon, G. E.; Haghighirad, A. A.; Martinez Hardigree, J.; Miranda, L.; Snaith, H. J.; Johnston, M. B.; Herz, L. M. *Nano Lett.* **2016**, *16*, 7001−7007.

(25) Wu, X. X.; Trinh, M. T.; Zhu, X. Y. *J. Phys. Chem. C* **2015**, *119*, 14714−14721.

(26) Straus, D. B.; Hurtado Parra, S.; Iotov, N.; Gebhardt, J.; Rappe, A. M.; Subotnik, J. E.; Kikkawa, J. M.; Kagan, C. R. *J. Am. Chem. Soc.* **2016**, *138*, 13798−13801.

(27) Guo, Z.; Wu, X.; Zhu, T.; Zhu, X.; Huang, L. *ACS Nano* **2016**, *10*, 9992−9998.

(28) Wu, K. F.; Liang, G. J.; Shang, Q. Y.; Ren, Y. P.; Kong, D. G.; Lian, T. Q. *J. Am. Chem. Soc.* **2015**, *137*, 12792−12795.

(29) Leng, J.; Liu, J.; Zhang, J.; Jin, S. *J. Phys. Chem. Lett.* **2016**, *7*, 5056−5061.

(30) Wu, X. X.; Trinh, M. T.; Niesner, D.; Zhu, H. M.; Norman, Z.; Owen, J. S.; Yaffe, O.; Kudisch, B. J.; Zhu, X. Y. *J. Am. Chem. Soc.* **2015**, *137*, 2089−2096.

DOI: 10.1021/jacs.6b12581
J. Am. Chem. Soc. 2017, 139, 1432−1435